ISA Transactions ■ (■■■■) ■■■–■■■

Contents lists available at ScienceDirect

ISA Transactions

journal homepage: www.elsevier.com/locate/isatrans

Research article

Control for delayed bilateral teleoperation of a quadrotor

E. Slawiński [1], D. Santiago [1], V. Mut [1]

Instituto de Automática, CONICET-Universidad Nacional de San Juan, Av. San Martín 1109 (O), San Juan 5400, Argentina

ARTICLE INFO

Article history:
Received 8 November 2016
Received in revised form
4 August 2017
Accepted 25 September 2017

Keywords:
Bilateral teleoperation
P+d controller
Time delay
Quadrotor

ABSTRACT

This paper proposes a cascade control scheme for delayed bilateral teleoperation of a quadcopter. The strategy transforms a 6D real quadcopter to an easy-to-teleoperate 3D virtual quadcopter. The scheme is formed by a P+d plus PID controller for each dof. The analysis based on Lyapunov theory gets as result the way to set the control parameters depending on the magnitude of the asymmetric time delays (forward and backward delays). This technic aims to reach stability, simplicity and good performance in practice. Besides, experimental tests about delayed bilateral teleoperation of a quadcopter including the proposed control scheme are shown in order to evaluate the system performance.

1. Introduction

The unmanned aerial vehicles (UAVs) allow avoiding the risk inherent for humans driving manned aerial vehicles, besides they are generally less expensive and smaller than their manned counterparts. Within UAVs, quadrotors have interesting flight capabilities to reach places and/or overfly specific areas such as hover, vertical take-off and landing, which cannot be achieved by conventional fixed-wing aircraft. These features make rotorcraft-like UAVs very useful for several tasks such as reconnaissance, rescue missions, inspection, surveillance and monitoring [1]. However, it is difficult to get a fully autonomous vehicle; so, the UAV teleoperation systems, where the human operator is included in the control loop, many times are more suitable for these missions [2]. Although there is a wide research in the area of UAVs for autonomous navigation (see [3] and references therein), few papers deal the stability analysis of a delayed bilateral teleoperation of a quadrotor-like UAV and the way suggested to calibrate the controller is currently an open topic. These systems have three parts: a ground station (local site), where a human operator receives information and drives a hand-controller device (master device); a UAV (slave vehicle or device) that receives control signals and flies through an environment (remote site) in order to perform some tasks; and a communication channel that links both sites. The haptic feedback allows coupling the human operator with the quadrotor and enhances his perception [4]. However, the communication channel adds delays that could cause instability or poor performance and low transparency [5,6]. For solve this, many control schemes, mainly addresed for delayed bilateral teleoperation systems of manipulators were proposed [7], in where the stability and/or passivity are analyzed [8]. For example, [9] and [10] use scattering and wave transformations to keep the passivity of the communication channel in front of time delay. These strategies inject the so called apparent damping, concept extended through the time-domain passivity approach (TDPA), formed by a Passivity Observer (PO) and Passivity Controller (PC) [11]. Furthermore, in [12,13], and [14] simple P+d schemes assure a stable teleoperation including position coordination. Besides, last classic scheme has been extended considering the actuators saturation [15] and also taking an adaptive SP+Sd-type (saturated proportion plus saturated damping) controller [16], based on an estimated velocity from an observer. In general, asymptotic stability is achieved using a sufficiently large damping injected into the master and slave, depending on the magnitude of the asymmetric time-varying delays. Recently, many interesting works have been proposed such as a terminal sliding mode (TSM)-based finite time control method [17], in which a finite-time synchronization performance is achieved, as well as control strategies based on neural networks applied to both bilateral and trilateral teleoperation [18,19], and adaptive fuzzy addressed to cooperative teleoperation of multiple manipulators [20].

On the other hand, the state-of-the-art for delayed teleoperation of mobile robots including force feedback [21] ranges different strategies, but in the last years the tendency is to adapt and apply the schemes used in manipulators teleoperation, such as control based on the r-passivity [22], energy-bounding approach [23], time domain passivity approach [24], and P (proportional) + d (damping) schemes robots [25], among others. Respect to delayed bilateral teleoperation of UAVs, the quantity of proposals including the corresponding theoretical analysis is even fewer. In [26–29] a

E-mail addresses: slawinski@inaut.unsj.edu.ar (E. Slawiński), dsantiago@inaut.unsj.edu.ar (D. Santiago), vmut@inaut.unsj.edu.ar (V. Mut).
[1] www.conicet.gov.ar; www.inaut.unsj.edu.ar

http://dx.doi.org/10.1016/j.isatra.2017.09.021
0019-0578/

bilateral teleoperation of multiple UAVs is performed by a single human operator and the stability is analyzed employing passivity theory. In the first two researches, the passivity of the master side is obtained applying feedback r-passivity notion [30]; then, it is claimed that the passivity of the teleoperation system can be easily enforced using any of the techniques developed in conventional teleoperation settings. In the latter two investigations, passive set-position modulation (PSPM) framework [31] is utilized to theoretically guarantee master passivity/VPs-stability of the closed-loop teleoperation system (where VPs refer to the virtual points followed by each UAV). In [32], a port-based modeling network is proposed. In particular, a port-Hamiltonian system is used including a variable impedance master controller and a virtual slave system, achieving passive teleoperation control architecture. Besides, in [33] a simple P+d controller is used to control a virtual delayed teleoperation system which is coupled with the real rotorcraft UAV from an elastic controller. Although the state-of-the-art about teleoperation systems is interesting and diverse, currently is an open topic select the best alternative to drive a quadrotor including time delay and force feedback.

From the context described above, a control scheme applied to delayed bilateral teleoperation of a quadrotor is proposed. The strategy combines in cascade both P+d and PID controllers. Besides, an easy-to-teleoperate virtual quadrotor that can be driven with only a 3 dof master is presented, which allows simplifying the human operator task. On the other hand, the force feedback improves the user perception about the synchronism error between master and slave, and helps him for generating sufficiently damped commands. It is important to remark that most commercial haptic devices have 3 dof, for which the proposed strategy is compatible with such devices available currently in the market. Also, the stability analysis of the closed control loop is carried out considering a dynamic master model, quadrotor dynamics, and asymmetric time-varying delays. In the current state-of-the-art is not clear how a control scheme addressed to these teleoperation systems must be calibrated. Instead in this work and as result of the theoretical analysis performed, guidelines to calibrate the controller, depending on the time delay, are proposed to achieve a stable control system applicable in practice for delayed bilateral teleoperation of a real UAV. The strategy is simple since adds a P+d controller layer over the current open source autopilots (PID in cascade like -ardupilot [34]). Finally, the control scheme is evaluated from experimental tests, where a human operator drives a quadrotor using a low-cost master device including force and visual feedback.

The paper is organized as follows: Section 2 presents some preliminary aspects such as the notation, employed dynamic models, properties and assumptions. In Section 3 and Appendix A, the control scheme is presented and the stability analysis is carried out, evaluating how the control parameters must be set depending on the time delay in order to assure stability. Section 4 shows human-in-the-loop tests where a user tele-operates, including time-varying delay, a 3D simulator and a real quadrotor in order to verify the achieved theoretical result. Finally, in Section 5 the conclusions of this work are given.

2. Preliminary

For analyzing the delayed bilateral teleoperation system of a quadrotor, let us introduce the models, assumptions, properties, and notation that will be used in this work. 1 shows the main parts of the system. It is important to remark that the communication channel adds a forward time delay h_1 (from the master to the slave) and a backward time delay h_2 (from the slave to the master), which are time-varying and generally different between them (asymmetric delays).

2.1. Notation

A standard notation throughout the paper is used but in order to clarify the mathematic procedure exposed in the next sections, some specific expressions are described. If x is a scalar, $\mathbf{w}$ is a vector and $\mathbf{Y}$ is a matrix, then, $|x|$ is the absolute value of x, $\mathbf{w}^T$ is the transpose of the vector, $\mathbf{Y}^T$ is the transpose of the matrix, $|\mathbf{x}|$ is the Euclidean norm of $\mathbf{x}$, $|\mathbf{Y}|$ is the induced norm of $\mathbf{Y}$, $\mathbf{Y} > 0$ ($\mathbf{Y} < 0$) means that $\mathbf{Y}$ is positive definite (negative definite). In addition, $\|\mathbf{w}\|_1$, $\|\mathbf{w}\|_2$ and $\|\mathbf{w}\|_\infty$ represent the $\mathcal{L}_1$ -norm, $\mathcal{L}_2$ -norm and $\mathcal{L}_\infty$ -norm of $\mathbf{w}$, respectively.

2.2. Models

In the local site, the master is located. A typical nonlinear dynamic model to represent a 3 dof master in Cartesian coordinates is used, which is described by,

$$\mathbf{M_m}(\mathbf{x_m})\ddot{\mathbf{x}}_m + \mathbf{C_m}(\mathbf{x_m}, \dot{\mathbf{x}}_m)\dot{\mathbf{x}}_m + \mathbf{g_m}(\mathbf{x_m}) = \mathbf{f_m} + \mathbf{f_h} \tag{1}$$

,where $\mathbf{x_m}(t), \dot{\mathbf{x}}_\mathbf{m}(t) \in \Re^3$ are the position and velocity of the robot in Cartesian coordinates, $\mathbf{M_m}(\mathbf{x_m})$ is the inertia matrix, $\mathbf{C_m}(\mathbf{x_m}, \dot{\mathbf{x}}_\mathbf{m})\dot{\mathbf{x}}_\mathbf{m}$ is the vector representing centripetal and coriolis forces, $\mathbf{g_m}(\mathbf{x_m})$ is the gravitational force, $\mathbf{f_h}$ is the force caused by the human operator and $\mathbf{f_m}$ is the control force applied to the master.

The slave vehicle (quadrotor) is placed on the remote site. It is represented by a multivariable system that has three translational (x, y, z) and three rotational (ϕ, θ, ψ) degrees of freedom (6 dof). It has four arms forming a cross, located at each end there is an actuator, formed by a motor and a propeller. Thus, quadrotor position and orientation is controlled by changing the speed at which the four rotors rotate. The general sketch of a quadrotor and reference frame is shown in Fig. 2.

A dynamic model of a quadrotor based on Lagrange Equations of Motion is considered [35], which is represented by,

$$\mathbf{D}^*\dot{\boldsymbol{\eta}}^* + \mathbf{Q}^*(\boldsymbol{\eta}^*)\boldsymbol{\eta}^* + \mathbf{g}^* = \boldsymbol{\tau}_\mathbf{s}^* + \mathbf{f}_\mathbf{e}^* \tag{2}$$

,where $\boldsymbol{\eta}^* = \begin{bmatrix} v_x & v_y & v_z & \omega_x & \omega_y & \omega_z \end{bmatrix}^T$ is the quadrotor velocity vector respect to a frame attached to the UAV, $\mathbf{f}_\mathbf{e}^*$ is the force caused by the elements of the environment on the robot such as the wind. Besides, the inertia matrix is represented by:

$$\mathbf{D}^* = \begin{bmatrix} m & 0 & 0 & 0 & 0 & 0 \\ 0 & m & 0 & 0 & 0 & 0 \\ 0 & 0 & m & 0 & 0 & 0 \\ 0 & 0 & 0 & I_{xx} & 0 & 0 \\ 0 & 0 & 0 & 0 & I_{yy} & 0 \\ 0 & 0 & 0 & 0 & 0 & I_{zz} \end{bmatrix} \tag{3}$$

,where m is the mass of the robot, and $I = \begin{bmatrix} I_{xx} & 0 & 0 \\ 0 & I_{yy} & 0 \\ 0 & 0 & I_{zz} \end{bmatrix}$ is the matrix including the inertial moments in each axis. The Coriolis matrix is expressed by:

$$\mathbf{Q}^* = \begin{bmatrix} 0 & -m\omega_z & m\omega_y & 0 & 0 & 0 \\ m\omega_z & 0 & -m\omega_x & 0 & 0 & 0 \\ -m\omega_y & m\omega_x & 0 & 0 & 0 & 0 \\ 0 & 0 & 0 & 0 & (I_{zz} - I_{yy})\omega_z & 0 \\ 0 & 0 & 0 & (I_{xx} - I_{zz})\omega_z & 0 & 0 \\ 0 & 0 & 0 & 0 & 0 & 0 \end{bmatrix} \tag{4}$$

Furthermore, the gravity vector has the following form:

Please cite this article as: Slawiñski E, et al. Control for delayed bilateral teleoperation of a quadrotor. ISA Transactions (2017), http://dx.doi.org/10.1016/j.isatra.2017.09.021

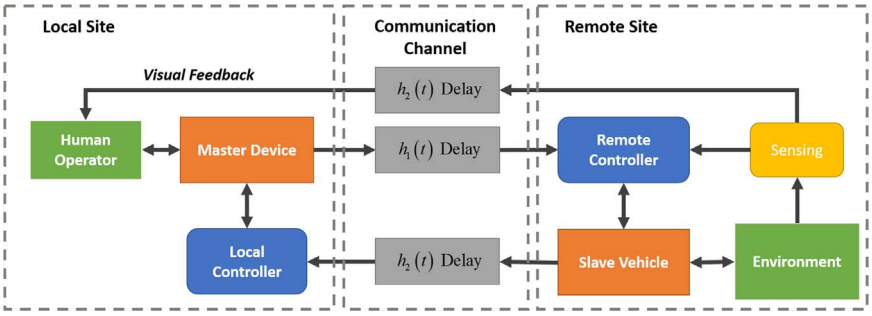

Fig. 1. General delayed teleoperation system.

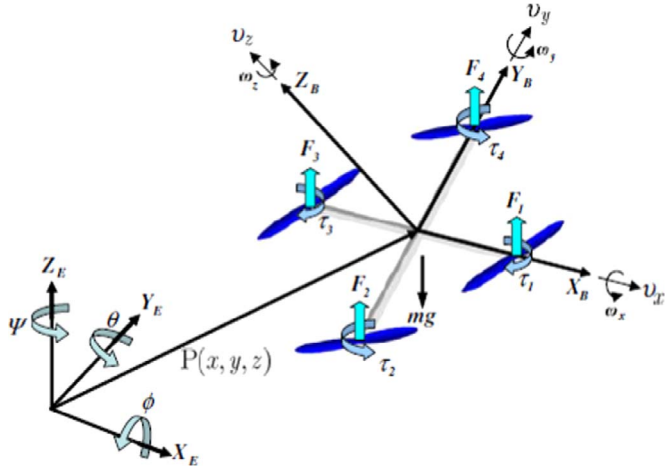

Fig. 2. Coordinate system of a quadrotor.

$$\mathbf{g}^* = \begin{bmatrix} -mg\sin\theta \\ mg\cos\theta\sin\varphi \\ mg\cos\theta\cos\varphi \\ 0 \\ 0 \\ 0 \end{bmatrix} \tag{5}$$

Where g is the gravity acceleration.

On the other hand, the control action is represented by $\boldsymbol{\tau}_s^* = [0\ 0\ u_1\ u_2\ u_3\ u_4]^T$ where u_1 is the total drag applied to the rotors, and u_2, u_3 and u_4 are the moments for pitch, roll and yaw, respectively. In practice, $\boldsymbol{\tau}_s^*$ is obtained driving the speed of four rotors as follows:

$$\begin{cases} u_1 = b\left(\Omega_1^2 + \Omega_2^2 + \Omega_3^2 + \Omega_4^2\right) \\ u_2 = bl\left(-\Omega_2^2 + \Omega_4^2\right) \\ u_3 = bl\left(-\Omega_1^2 + \Omega_3^2\right) \\ u_4 = d\left(-\Omega_1^2 + \Omega_2^2 - \Omega_3^2 + \Omega_4^2\right) \end{cases} \tag{6}$$

Where Ω_1, Ω_2, Ω_3, Ω_4 are the angular speed for the rotors, b is the drag factor, d is the drag coefficient and l is the distance between the center of mass and the rotor. From now on, the vector $\mathbf{u} = [u_1\ u_2\ u_3\ u_4]^T$ represents the control action that will be applied to the quadrotor (Fig. 1).

2.3. Assumptions and properties

The following ordinary properties, assumptions and lemmas will be used in this paper [8,11]:

Property 1. *The inertia matrices* $\mathbf{M_m}(\mathbf{x_m})$ *and* $\mathbf{D}^*$ *are symmetric positive definite.*

Property 2. *The matrix* $\dot{\mathbf{M}}_\mathbf{m}(\mathbf{x_m}) - 2\mathbf{C_m}(\mathbf{x_m}, \dot{\mathbf{x}}_\mathbf{m})$ *is skew-symmetric.*

Property 3. *There exists a* $k_r > 0$ *such that* $\left|\mathbf{C_m}(\mathbf{x_m}, \dot{\mathbf{x}}_\mathbf{m})\dot{\mathbf{x}}_\mathbf{m}\right| \le k_r \left|\dot{\mathbf{x}}_\mathbf{m}\right|^2$ *for all time* t.

Property 4. *The vector* $\mathbf{g_m}(\mathbf{x_m})$ *is bounded if* $\mathbf{x_m}$ *is bounded.*

Assumption 1. The time delays $h_1(t)$ and $h_2(t)$ are bounded. Therefore, there exist positive scalars $\bar{h}_1$ and $\bar{h}_2$ such that $0 \le h_1(t) \le \bar{h}_1$ and $0 \le h_2(t) \le \bar{h}_2$ for all t.

Assumption 2. The human operator has finite-energy [8] and the environment is represented by a damping-like model plus a finite-energy perturbation [14]. Such models are mathematically represented as follows:

$$E_h = \varphi_h - \int_0^t \mathbf{f}_\mathbf{h}^T \dot{\mathbf{x}}_\mathbf{m} dt \ge 0 \tag{7}$$

$$\mathbf{f_e} = -\alpha_e \boldsymbol{\eta}^* + \mathbf{f_{a_e}} \tag{8}$$

,where $\mathbf{f_h}$ is the human force, $\varphi_h > 0$ is a finite value that bounds the energy of the human operator, α_e is the environments damping, and $\mathbf{f_{a_e}}$ is assumed bounded with finite energy and bounded derivative, that is $\left|\mathbf{f_{a_e}}\right| \le \bar{f}_{a_e}$ with $\bar{f}_{a_e}$ a positive constants and $\mathbf{f_{a_e}} \in \mathcal{L}_2$. **Lemma 1** [13]: For vector functions $\mathbf{a}(\cdot)$ and $\mathbf{b}(\cdot)$ and a time-varying scalar $h(t)$ with $0 \le h(t) \le \bar{h}$, the following inequality holds,

$$-2\mathbf{a}^T(t)\int_{t-h(t)}^t \mathbf{b}(\xi)d\xi - \int_{t-h(t)}^t \mathbf{b}^T(\xi)\mathbf{b}(\xi)d\xi \le h(t)\mathbf{a}^T(t)\mathbf{a}(t) \le \bar{h}(t)\mathbf{a}^T(t)\mathbf{a}(t) \tag{9}$$

3. Proposed control scheme

In this section, a control scheme is proposed for bilateral teleoperation of a quadcopter in presence of time delay including force feedback to the user. Fig. 3 shows a general diagram of the controller proposed. Many strategies proposed in the literature use a virtual model coupled with the real UAV, which facilities the analysis but at cost of adding some double dynamics into the teleoperation system and makes the transparency worse. In particular, the force feedback generally does not represent some real force of the quadcopter. On the other hand, most autopilots include a structure formed by PID controllers in cascade for the gaz, pitch, roll and yaw rate, which works well in practice. But, to the best knowledge of the authors, this type of strategy or similar have

Please cite this article as: Slawiñski E, et al. Control for delayed bilateral teleoperation of a quadrotor. ISA Transactions (2017), http://dx.doi.org/10.1016/j.isatra.2017.09.021

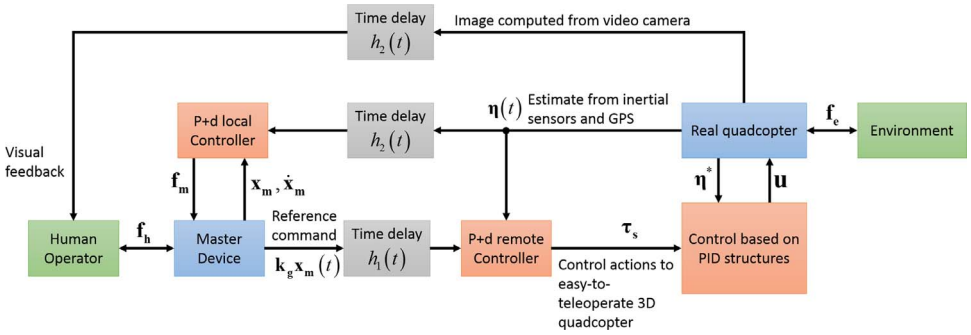

Fig. 3. Diagram of the proposed control scheme.

not been formalized for its application in delayed bilateral teleoperation of a quadcopter.

The proposal of this paper consists of standard control schemes combined in cascade. On the one hand, P+d controllers are applied in an external loop to a simplified 3D model while PID-like controllers are used in an internal loop in order to achieve that the real quadrotor plus the PID control scheme behaves as the mentioned simplified model. This whole control scheme has as output the control actions that will be applied to the real quadrotor. Next, the stability of the external control loop will be studied in this section in order to analyze the use and calibration of the proposed control scheme.

P+d controllers are simple structures that generally have a good performance in practice for several applications including bilateral teleoperation systems of manipulator robots [12–14] as well as bilateral teleoperation of mobile robots [25] and mobile manipulators [36]. To apply this control type to a real quadrotor, a cascade structure formed by two control loops (external and internal loops) is proposed. The external loop will be applied to an easy-to-teleoperate 3 dof virtual quadrotor, whose model is proposed as follows:

$$\mathbf{D}\dot{\boldsymbol{\eta}} = \boldsymbol{\tau}_s + \mathbf{f}_e \tag{10}$$

Where $\mathbf{D} = \begin{bmatrix} m & 0 & 0 \\ 0 & m & 0 \\ 0 & 0 & I_{zz} \end{bmatrix}$, $\dot{\eta} = \begin{bmatrix} \dot{v}_x \\ \dot{v}_z \\ \dot{\omega}_z \end{bmatrix}$ and $\boldsymbol{\tau}_s = \begin{bmatrix} u_{x_{virtual}} \\ u_{1_z} \\ u_4 \end{bmatrix}$.

Next, the P+d scheme applied to (1) and (10) is formed by $\mathbf{f_m}$ (force feedback to the user) and $\boldsymbol{\tau_s}$ (control action applied to the virtual quadrotor) which are established as follows:

$$\mathbf{f_m} = -k_m\left(k_g\mathbf{x_m} - \boldsymbol{\eta}(t-h_2)\right) - \alpha_m\dot{\mathbf{x}}_\mathbf{m} - k_p\mathbf{x_m} + \mathbf{g_m}(\mathbf{x_m}) \tag{11}$$

$$\boldsymbol{\tau_s} = k_s\left(k_g\mathbf{x_m}(t-h_1) - \boldsymbol{\eta}\right) - \sigma_s\mathbf{z} \tag{12}$$

Where the parameter k_s is a positive constant value that represents a proportional gain of a velocity controller applied to the quadrotor, k_m represents a scaling gain to map the velocity error between master and quadrotor into the force range of the master, k_g is a positive constant value which linearly maps the master position to a velocity reference $k_g\mathbf{x_m} = \begin{bmatrix} v_{x_{ref}} & v_{z_{ref}} & \omega_{z_{ref}} \end{bmatrix}^T$, k_p is an elastic coefficient of spring included in the master, and α_m and σ_s are controlled coefficients of damping and acceleration-damping injected in the master and quadrotor, respectively. Besides, a signal $\mathbf{z} = \begin{bmatrix} z_{v_x} & z_{v_z} & z_{\omega_x} \end{bmatrix}^T$ is used which represents the quadrotor acceleration $\dot{\boldsymbol{\eta}}$ at an infinitesimal time instant before t, that is

$$\dot{\boldsymbol{\eta}} = \mathbf{z} + \gamma\, k_z \tanh\left(\frac{1}{k_z}\dot{\mathbf{z}}\right) \tag{13}$$

With $\gamma \to 0^+$ and $k_z > 0$. In practice, $\mathbf{z}$ generally is related with the output of inertial sensors such as the signals provided by an Inertial Measurement Unit (IMU).

Remark 1. The parameters k_g, k_p, k_m, k_s, α_m, σ_s are taken as scalar only to simplify the notation, but in general they can be diagonal matrices called $\mathbf{K_g}$, $\mathbf{K_p}$, $\mathbf{K_m}$, $\mathbf{K_s}$, $\boldsymbol{\alpha}_\mathbf{m}$, $\boldsymbol{\sigma}_\mathbf{s}$ respectively.

3.1. Stability analysis

First, a positive definite functional $V\left(\mathbf{x_m}, \dot{\mathbf{x}}_\mathbf{m}, k_g\mathbf{x_m} - \boldsymbol{\eta}, \boldsymbol{\eta}, \dot{\boldsymbol{\eta}}, \mathbf{z}\right) = V_1 + V_2 + V_3 + V_4 + V_5 + V_6$ will be defined to analyze its evolution along the system trajectories. It is assumed that the initial condition is finite. The functional is formed by six parts, where V_6 is included to convert the terms including delayed variables to terms with non-delayed variables. The sub-functional V_i are proposed of the following manner:

$$V_1 = \frac{1}{2}\dot{\mathbf{x}}_\mathbf{m}^T\mathbf{M_m}(\mathbf{x_m})\dot{\mathbf{x}}_\mathbf{m} + E_h \tag{14}$$

$$V_2 = \frac{1}{2}\frac{k_m}{k_g}\left(k_g\mathbf{x_m} - \boldsymbol{\eta}\right)^T\left(k_g\mathbf{x_m} - \boldsymbol{\eta}\right) \tag{15}$$

$$V_3 = \frac{1}{2}\frac{\alpha_e k_m}{k_s k_g}\boldsymbol{\eta}^T\boldsymbol{\eta} \tag{16}$$

$$V_4 = \frac{1}{2}\frac{k_m}{k_s k_g}\int \dot{\boldsymbol{\eta}}^T\mathbf{D}\dot{\boldsymbol{\eta}} \tag{17}$$

$$V_5 = \frac{1}{2}k_p\mathbf{x}_\mathbf{m}^T\mathbf{x_m} \tag{18}$$

$$V_6 = k_m\int_{-h_2}^{0}\int_{t+\theta}^{t}\mathbf{z}(\xi)^T\mathbf{z}(\xi)d\xi d\theta + k_m\int_{-h_1}^{0}\int_{t+\theta}^{t}\dot{\mathbf{x}}_\mathbf{m}(\xi)^T\dot{\mathbf{x}}_\mathbf{m}(\xi)d\xi d\theta \tag{19}$$

Next, $\dot{V}$ is obtained applying Appendix A to (14), (15), (16), (17), (18) and (19), getting as result the following:

$$\begin{aligned}\dot{V} &= \dot{V}_1 + \dot{V}_2 + \dot{V}_3 + \dot{V}_4 + \dot{V}_5 + \dot{V}_6 \\ &\le \dot{\mathbf{x}}_\mathbf{m}^T\left[-\alpha_m\mathbf{I} + k_m h_1\mathbf{I} + \frac{k_m}{4}h_2\mathbf{I}\right]\dot{\mathbf{x}}_\mathbf{m} \\ &\quad + \mathbf{z}^T\left[-\sigma_s\frac{k_m}{k_s k_g}\mathbf{I} + k_m h_2\mathbf{I} + \frac{k_m}{4}h_1\mathbf{I} + \frac{k_m^2}{4k_g^2k_s^2}\mathbf{I}\right]\mathbf{z} + \mathbf{f}_{\mathbf{a_e}}^T\mathbf{f}_{\mathbf{a_e}}\end{aligned} \tag{20}$$

Now, if the integral between 0 and t is applied over (20), the following expression is get:

$$V(t) - V(0) \leq -\lambda_1 \left\|\dot{\mathbf{x}}_\mathbf{m}\right\|_2 - \lambda_2 \left\|\mathbf{z}\right\|_2 + \left\|\mathbf{f}_{\mathbf{a_e}}\right\|_2 \tag{21}$$

Where:

$$\begin{cases} \lambda_1 = \alpha_m - k_m h_1 - \dfrac{k_m}{4} h_2 \\ \lambda_2 = \sigma_s \dfrac{k_m}{k_s k_g} - k_m h_2 - \dfrac{k_m}{4} h_1 - \dfrac{k_m^2}{4 k_g^2 k_s^2} \end{cases} \tag{22}$$

Result 1. From (21), if the damping coefficients α_m and σ_s are sufficiently high such that $\lambda_1, \lambda_2 > 0$, then:

$$V(t) \leq V(0) + \left\|\mathbf{f}_{\mathbf{a_e}}\right\|_2 \tag{23}$$

That is, since $\mathbf{f}_{\mathbf{a_e}} \in \mathcal{L}_2$ (Assumption 2), and the functional $V\left(\mathbf{x}_\mathbf{m}, \dot{\mathbf{x}}_\mathbf{m}, k_g \mathbf{x}_\mathbf{m} - \boldsymbol{\eta}, \boldsymbol{\eta}, \dot{\boldsymbol{\eta}}, \mathbf{z}\right)$ is radially unbounded and from (23), it is bounded along the system trajectories for all t; then $\mathbf{x}_\mathbf{m}, \dot{\mathbf{x}}_\mathbf{m}, k_g \mathbf{x}_\mathbf{m} - \boldsymbol{\eta}, \boldsymbol{\eta}, \dot{\boldsymbol{\eta}}, \mathbf{z} \in \mathcal{L}_\infty$. Even more, considering this result into (21), it yields:

$$\lambda_1 \left\|\dot{\mathbf{x}}_\mathbf{m}\right\|_2 + \lambda_2 \left\|\mathbf{z}\right\|_2 \leq \left\|\mathbf{f}_{\mathbf{a_e}}\right\|_2 + V(0) \tag{24}$$

In this way, the variables $\dot{\mathbf{x}}_\mathbf{m}, \mathbf{z} \in \mathcal{L}_2$.

Corollary 1. *From (11) and (12) the control actions applied to the virtual quadrotor and force feedback for the human operator, can be expressed by* $\boldsymbol{\tau}_\mathbf{s} = k_s\left(k_g \mathbf{x}_\mathbf{m}(t) - \boldsymbol{\eta}\right) - k_s k_g \int_{t-h_1}^{t} \dot{\mathbf{x}}_\mathbf{m}(\xi) d\xi - \sigma_s \mathbf{z}$ *and* $\mathbf{f}_\mathbf{m} = -k_m\left(k_g \mathbf{x}_\mathbf{m} - \boldsymbol{\eta}(t - h_2)\right) - k_m \int_{t-h_2}^{t} \dot{\boldsymbol{\eta}}(\xi) d\xi - \alpha_m \dot{\mathbf{x}}_\mathbf{m} - k_p \mathbf{x}_\mathbf{m} + \mathbf{g}_\mathbf{m}(\mathbf{x}_\mathbf{m})$. *Using Result 1, this is:* $\mathbf{x}_\mathbf{m}, \dot{\mathbf{x}}_\mathbf{m}, k_g \mathbf{x}_\mathbf{m} - \boldsymbol{\eta}, \boldsymbol{\eta}, \dot{\boldsymbol{\eta}}, \mathbf{z} \in \mathcal{L}_\infty$, *then both* $\boldsymbol{\tau}_\mathbf{s} = \left[u_{x_{virtual}} \;\; u_{1_z} \;\; u_4\right]^T$ *and* $\mathbf{f}_\mathbf{m} \in \mathcal{L}_\infty$ *too.*

Result 2. From (20), if α_m, σ_s are greater then $\dot{\mathbf{x}}_\mathbf{m}, \mathbf{z}$ (master velocity and slave acceleration) will tend to a smaller convergence ball.

Corollary 2. *If* $\mathbf{f}_\mathbf{h}$ *and* $\mathbf{f}_{\mathbf{a_e}}$ *are null then the following situation will occur: From* Result 1, **Properties 3, 4** *and* Assumption 2, *the terms* $\left|\mathbf{C}_\mathbf{m}(\mathbf{x}_\mathbf{m}, \dot{\mathbf{x}}_\mathbf{m})\dot{\mathbf{x}}_\mathbf{m}\right|$, $\left|\mathbf{g}_\mathbf{m}(\mathbf{x}_\mathbf{m})\right|$, *and* $\mathbf{f}_\mathbf{e}$ *are bounded. Besides, taking into account* Corollary 1 ($\mathbf{f}_\mathbf{m}, \boldsymbol{\tau}_\mathbf{s} \in \mathcal{L}_\infty$) *and* Property 1, *it is possible to state that* $\ddot{\mathbf{x}}_m$ (1) *and* $\dot{\boldsymbol{\eta}}$ (10) *are bounded too. From this,* $\dot{V} \in \mathcal{L}_\infty$(*evaluating the derivative of* (20)). *Next, Barbalat lemma is applied getting* $\dot{V} \to 0$ *and therefore,* $\dot{\mathbf{x}}_\mathbf{m}, \mathbf{z} \to \mathbf{0}$ ($\dot{\boldsymbol{\eta}} \to \mathbf{0}$ *from* (13)) *as* $t \to \infty$.

Remark 2. In P+d control schemes, if the damping level is greater, then the transparency gets worse [6,13]. Currently it is an open topic to use different techniques such as optimization methods, to get better numerical conditions in order to achieve a stable delayed teleoperation system keeping the higher transparency level possible.

3.2. Control actions applied to the 6D real quadrotor

The stability analysis performed in last section assumes that the real quadrotor can be represented by the model presented in (10). However, the proposal includes a control structure in cascade of way that the internal loop will search to obtain a behavior similar to such simplified model, while the external loop is designed in (11) and (12) to get a stable response and bounded error of the delayed bilateral teleoperation system. From (2) to (5), the quadrotor dynamic model in state space can be expressed with the following six equations of motion:

$$\begin{aligned} m\left[\dot{v}_x - v_y\omega_z + v_z\omega_y - g\sin\theta\right] &= 0 \\ m\left[\dot{v}_y - v_z\omega_x + v_x\omega_z + g\cos\theta\sin\varphi\right] &= 0 \\ m\left[\dot{v}_z - v_x\omega_y + v_y\omega_x + g\cos\theta\cos\varphi\right] &= u_1 \end{aligned} \tag{25}$$

$$\begin{aligned} I_{xx}\dot{\omega}_x + \left(I_{zz} - I_{yy}\right)\omega_y\omega_z &= u_2 \\ I_{yy}\dot{\omega}_y + \left(I_{xx} - I_{zz}\right)\omega_z\omega_x &= u_3 \\ I_{zz}\dot{\omega}_z &= u_4 \end{aligned}$$

On the other hand, the virtual model expressed in (10) without the environment force $\mathbf{f}_\mathbf{e}$, can be represented with the following three equations of motion:

$$\begin{aligned} m\dot{v}_x &= u_{x_{virtual}} \\ m\dot{v}_z &= u_{1_z} \\ I_{zz}\dot{\omega}_z &= u_4 \end{aligned} \tag{26}$$

Now, the calculus of u_1, u_2, u_3, u_4 is carried out in order to apply them to the real quadrotor (25). First, comparing the third row of (25) with the second row of (26), it is possible to get:

$$u_1 = u_{1_z} + m v_y \omega_x - m v_x \omega_y + mg\cos\theta\cos\varphi \tag{27}$$

The control action u_1 includes compensation of both gravity and Coriolis force. A non-exact or unavailable compensation of Coriolis forces and gravity cause velocity tracking errors, which are decreased in practice by the commercial autopilots adding an integral control part, that is: $u_1 = u_{1_z} + k_i \int\left(v_{z_{ref}} - v_z\right)dt$. On the other hand, the easy-to-teleoperate quadrotor (26) has fewer dof than the real one (25). Specifically, the lateral motion is restricted so lateral velocity reference is set to $v_{y_{ref}} = 0$. A cascade PID structure is used to keep v_y near to zero, that is u_2 is computed by:

$$\begin{aligned} u_2 &= PID\left(\varphi_{ref} - \varphi\right) \\ \varphi_{ref} &= PID\left(v_{y_{ref}} - v_y\right) \end{aligned} \tag{28}$$

Besides, u_3 is controlled to drive the pitch θ such that the velocity v_x be as close as possible to the velocity reference. Comparing the first row of both (25) and (26), the following expression is obtained:

$$m\dot{v}_x = -m v_z\dot{\theta} + m v_y\omega_z + mg\sin\theta = u_{x_{virtual}} \tag{29}$$

Now, considering in (29) $v_y \approx 0$ from (28), and $\theta \approx \sin\theta$ (valid for small angles which is common for most flights), the following expression to represent the reference θ_{ref} of the pitch angle is proposed:

$$\theta_{ref} = \frac{u_{x_{virtual}}}{mg} \tag{30}$$

Next, the control action proposed for u_3 is computed by a PID controller plus Coriolis compensation, as follows:

$$\begin{aligned} u_3 &= k_{p_3}\left(\theta_{ref} - \theta\right) - k_{d_3}\dot{\theta} + k_{i_3}\int_0^t \left(\theta_{ref} - \theta\right)dt \\ &\quad + \left(I_{xx} - I_{zz}\right)\omega_z\omega_x + k_{i_3}\int_0^t \frac{1}{g} v_z\dot{\theta}dt \end{aligned} \tag{31}$$

where the pitch is generally computed from a Kalman filter applied to the IMU data and the angular velocities such as $\omega_y = \dot{\theta}$, are measured commonly using a 3D gyroscope sensor. In practice, most open source autopilots use two PID controllers in cascade instead of applying Coriolis compensation. Replacing u_3 of (31) in the fifth row of the quadrotor dynamics (25), we get:

Please cite this article as: Slawiñski E, et al. Control for delayed bilateral teleoperation of a quadrotor. ISA Transactions (2017), http://dx.doi.org/10.1016/j.isatra.2017.09.021

$$I_{yy}\ddot{\theta} = k_{p_3}\left(\theta_{ref} - \theta\right) - k_{d_3}\dot{\theta} + k_{i_3}\int_0^t \left(\theta_{ref} - \theta\right)dt + k_{i_3}\int_0^t \frac{1}{g}v_z\dot{\theta}dt \tag{32}$$

Deriving both sides of (32), and then applying the Laplace transform, it is possible to get:

$$\theta(s) = \frac{\left(\frac{k_{p_3}}{k_{i_3}}s + 1\right)}{D(s)}\theta_{ref}(s) + \frac{v_z}{g}\frac{1}{D(s)}\dot{\theta}(s) \tag{33}$$

Where

$$D(s) = \frac{I_{yy}}{k_{i_3}}s^3 + \frac{k_{d_3}}{k_{i_3}}s^2 + \frac{k_{p_3}}{k_{i_3}}s + 1 \tag{34}$$

The parameters k_{p_3}, k_{d_3} and k_{i_3} can be set to assure that $D(s)$ has all roots with negative real part and a fast transitory response. Assuming this condition, Eq. (34) can be represented of the following manner:

$$\theta(t) = \theta_{ref}(t) + \frac{1}{g}v_z(t)\dot{\theta}(t) + p(t) \tag{35}$$

Where the error p is negligible in practice since the transitory response of $D(s)$ can be arbitrarily established from setting the PID parameters. Furthermore, if (35) is inserted into (29), considering $v_y \approx 0$, $\theta \approx \sin\theta$, $p \approx 0$ and relation (30), then the following result is obtained:

$$\begin{aligned} m\dot{v}_x &= -mv_z\dot{\theta} + mg\theta \\ &= -mv_z\dot{\theta} + mg\left(\theta_{ref} + \frac{v_z\dot{\theta}}{g}\right) \\ &= -mv_z\dot{\theta} + mg\left(\frac{u_{x_{virtual}}}{mg} + \frac{v_z\dot{\theta}}{g} + p\right) \\ &= u_{x_{virtual}} \end{aligned} \tag{36}$$

As result, Equation (36) is compatible with the first raw of (26). Finally, the dynamics of the easy-to-teleoperate model and real one are similar on last rows of (25) and (26) and therefore, u_4 can be established from (12).

Result 3. If the internal control loop applied to the real quadrotor is formed by Eq. (27) for u_1, (28) for u_2, and (31) for u_3 then the quadrotor plus the internal control loop, behaves in a way similar to the easy-to-teleoperated quadrotor defined in (10).

Result 4. From the theoretical results achieved, the following guidelines are recommended to calibrate the proposed control scheme: **(a)** Set the parameters of the internal control loop without time delay, that is calibrate the PID-like controllers, presented in (27), (28) and (31), like the common autopilots; **(b)** Adjust the independent parameters of the external control loop given in (11) and (12) for null delay, taking the possible minimum value for α_m, σ_s. Here, the calibration criterion is to get a good velocity tracking responding to the master commands; and **(c)** Set the damping coefficients α_m and σ_s depending on the time delay considering the parameters selected in step **(d)** for assuring sufficiently slow motions of the master and slave (quadrotor) in order to retain the system stability.

4. Experimental results

In this section, the proposed control scheme is evaluated experimentally with a 3D UAV simulator as well as using a real quadcopter. In the testing, a human operator teleoperates a real or simulated quadcopter receiving visual and force feedback. Furthermore, to implement the teleoperation system, the following tools are used: MATLAB/Simulink from www.mathworks.com running with the real-time module, and the SAS library from https://drive.google.com/drive/folders/0B2jklwyyOJqPNVA2SWFSaGFSNnc?usp=sharing, V-REP simulation environment (http://www.coppeliarobotics.com), the Ardrone Parrot model quadrotor https://www.parrot.com/ and a low-cost manipulator (master), Novint Falcon model http://www.novint.com, which has 3 dof including force feedback. In the case of the simulated quadrotor, its dynamic is programmed using a toolbox of robotics available in http://www.petercorke.com and the framework Vrep, while that the ardrone parrot is used for the real tests.

The built-in implementation easily allows doing tests with a simulated or real quadcopter as it is illustrated in Fig. 4.

The tests are divided into two parts: A) A human operator drives a 3D simulator of a quadrotor; and B) A human operator drives a Ardrone Parrot quadrotor. The test A has as goal to carry out an experiment sufficiently structured (using a 3D quadrotor simulator) to get as result an adequate comparison between the P+d-PID control scheme including a damping sufficiently high to assure stability and a P-PID controller (without damping). On the other hand, the test B is addressed to evaluate the behavior in practice (real quadrotor) of the P+d-PID control scheme as the delay increases. In both tests type, some common performance indexes will be used as comparison tool.

4.1. Test A

The task assigned to the human operator, consists of driving a simulated quadrotor for passing through 3D points from an initial position to a target position in a given sequence. The point at which the operator must steer the aircraft is illuminated in green in order to point out the path that the quadrotor must follow. See Fig. 5.

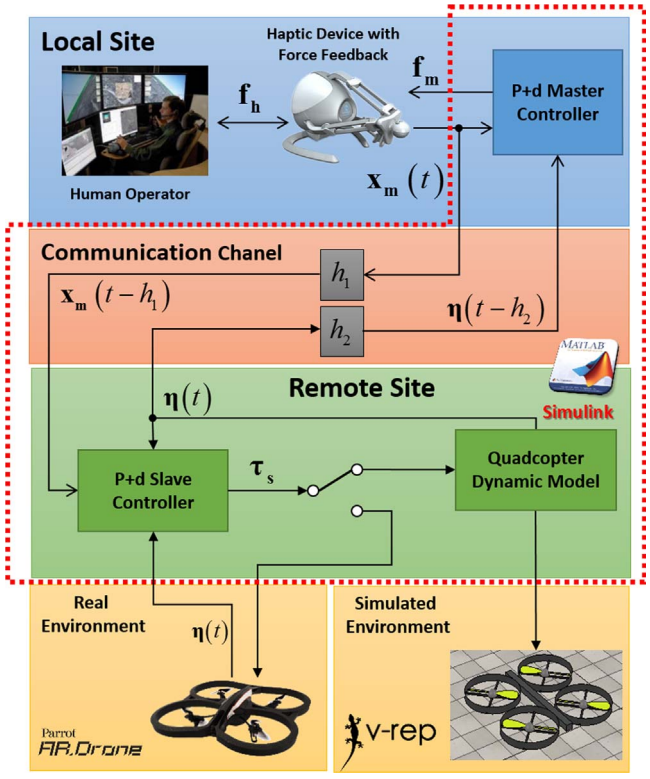

Fig. 4. Experimental setup scheme for tests.

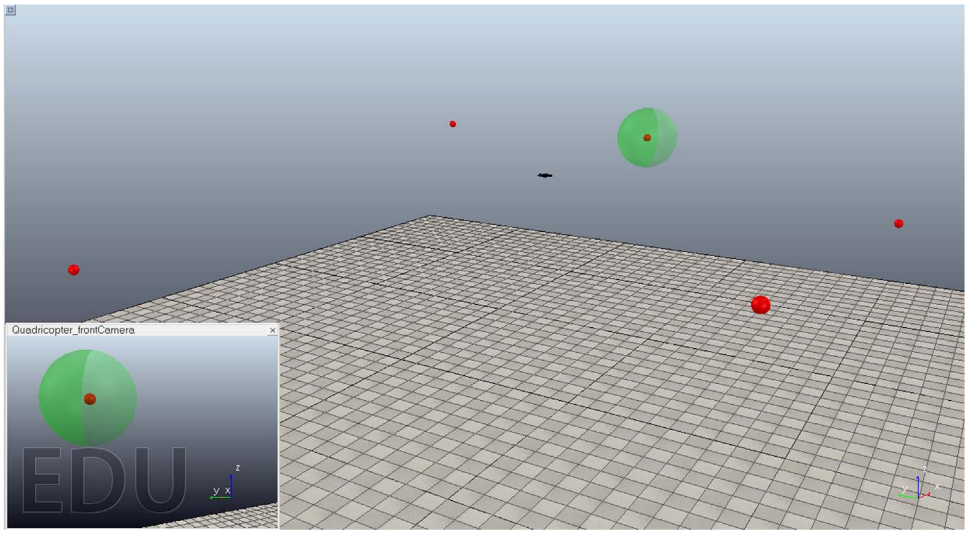

Fig. 5. quadrotor should navigate through 3D points marked in green.

At the outset tests are performed without time delay, in order to choose a reference pattern. Then the performance is evaluated comparing the pattern chosen with the performance achieved for three different simulated time delays, which are established arbitrarily as follows:

$$\text{Delay1: } \begin{cases} h_1 = 0.1 + 0.1\sin(4t + 0.1) \\ h_2 = 0.2 + 0.1\sin(t + 0.5) \end{cases}$$

$$\text{Delay2: } \begin{cases} h_1 = 0.2 + 0.1\sin(3t + 0.3) \\ h_2 = 0.5 + 0.2\sin(t + 0.5) \end{cases}$$

$$\text{Delay3: } \begin{cases} k_j = 1.0 + 0.5\sin(2t + 0.4) \\ h_2 = 0.7 + 0.3\sin(t + 0.5) \end{cases}$$

In order to evaluate the performance obtained, the response of the teleoperation system in front of both a good calibration and a non-adequate setting, is compared for different time delays. In last calibration type, a minimal damping into the slave is considered and a null damping is used in the master. On the other hand, the calibration based on the achieved theoretical result is carried out taking into account the guidelines described in Result 4. This is, the parameters independent from the time delay are calibrated empirically to get a good performance without time delay (reference pattern). Then, the damping coefficients on the slave and master must be increased as the time delay is higher. Since the Novint Falcon master device has a low force range, the highest damping value that works well in practice was used. Such control parameter is set to $\alpha_m = 1.2[\,Kg/s\,]$.

For the performance measurement, the spatial correlation between the ideal path (straight line between targets) and the path followed by the quadrotor, is quantified as follows:

$$\beta = \sum_{i=1}^{n} \min_{k_j \subset [1, m_j]} \left(\left\| \mathbf{r}(i) - \mathbf{p_j}(k_j) \right\| \right)$$

,where $\mathbf{r}_i$ is the optimal 3d path, for $i \subset [1, n]$ being n the total points of such path, $\mathbf{p_j}(k)$ is the 3D path followed by the quadrotor for each j-experiment, and m_j is the points total quantity of the j-path.

The results of the experiment are summarized on Table 1, where the performance index β is computed for different time delays considering both a good calibration and a non-adequate setting. For higher time delays the performance of the task decreases. The damping injected into the system improves the performance in all cases with exception of the case without time delay, where the damping hinders the task. Fig. 6 shows the effect of the damping injection on the quadcopter path. It is important to remark that higher time delays produces greater errors between the ideal and the real path followed by the quadcopter and also abrupt fluctuations along the trayectory.

Table 1
Results about β index.

	Non delay	Delay 1	Delay 2	Delay 3
$\alpha_m = 0$	0.6	0.7	0.96	1.0
$\alpha_m = 1.2$	0.63	0.66	0.71	0.81

4.2. Test B

In order to verify a stable behavior in practice, a test of networked bilateral teleoperation driving a quadcopter (ardrone parrot model) without sight line and time delay, is performed. The Fig. 7 shows an images sequence of the test setup, in which the task given to the user, is to make a visual inspection of the type-cylinder object hanging on the ceiling, from a quadcopter initial pose and then back to it. An Ethernet network is used to communicate the quadcopter with the master device. In addition, a round trip delay about 1 second is added to the delay caused by the local network. The video acquired by the camera onboard the quadcopter is back-feed to the user as well as force feedback depending on the synchronization error and damping injected.

Figs. 8 and 9 show the time delay measured during the test, the evolution of velocity references (measured in the local site) and the velocities of the quadrotor (measured in the remote site). In the last figure, the subplots correspond to v_x, v_y, v_z, ω_z and their respective references that must be followed.

In the link https://youtu.be/o8yGarNis8w, the video of the test can be visualized. The result achieved in practice is in agreement with the theoretical result in the sense that the error between master and slave (quadrotor) remains bounded in spite of the time-varying delay added by the communication channel. Next, the experimental setup is repeated 10 times for different time delays. First, a base test is performed where no delay is added to the communication channel. Then, three tests are performed: low

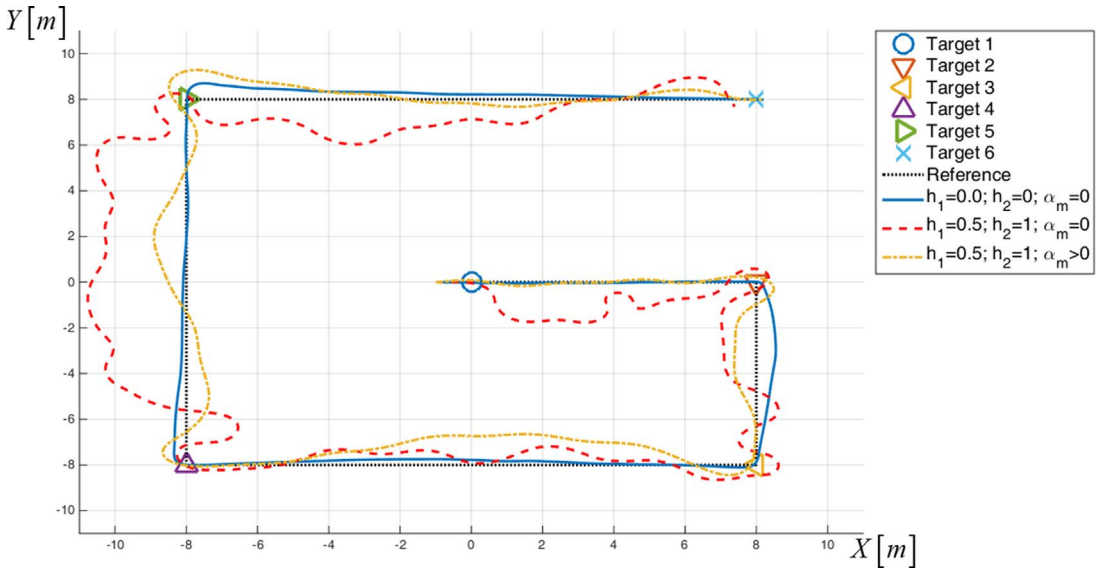

Fig. 6. Trajectories achieved for different delays and damping.

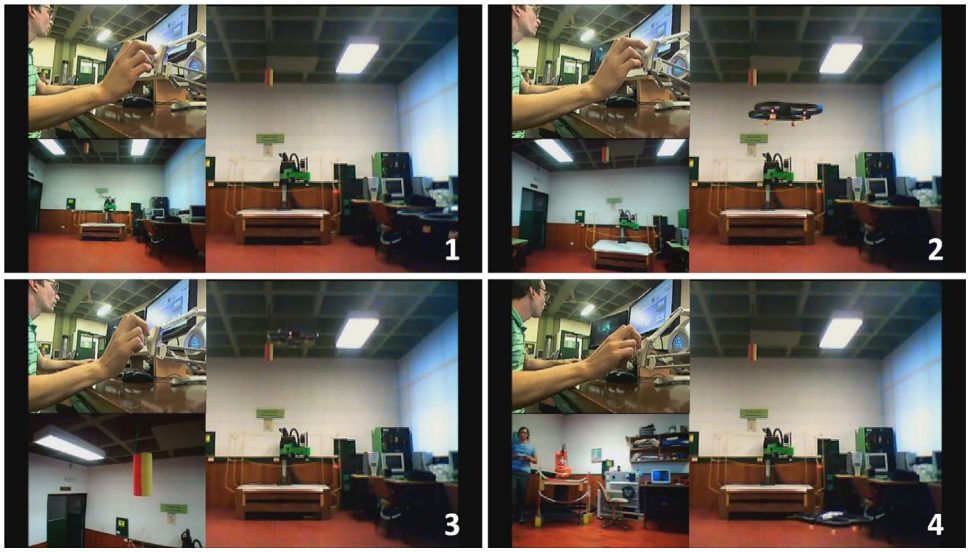

Fig. 7. Experimental setup.

delay ($\bar{h}_1 = 0.4, \bar{h}_2 = 0.2$), medium delay ($\bar{h}_1 = 0.5, \bar{h}_2 = 0.7$) and high delay ($\bar{h}_1 = 1, \bar{h}_2 = 1$). For each delay, the controller is calibrated for each case; in particular the damping is increased as the time delay is higher according to Result 4. The performance is measured with two different indexes: $I_{sync} = \int_0^{T_{task}} \left[\mathbf{x_m}(t) - \boldsymbol{\eta}(t) \right] dt$ which measures the synchronization error between the master robot and slave throughout the test, and time to complete the task (T_{task}). The results are presented in Table 2, where the obtained data are expressed in percentage respect to the base test (without time delay).

The performance of the delayed teleoperation system, with respect to the time to complete the task, degrades as the time delay increase. Besides, the index about synchronism error between master and quadcopter also gets worse. However, it is important to remark that the inspection task goal was completed in all tests, keeping a bounded synchronism error which is in agreement with the achieved theoretical result. From a practical view point, the performance is satisfactory until a middle delay (about 1.2 s of round-trip delay) since the task time increases only 7.7%. This motivates the use of the proposed control scheme addressed to different application fields.

5. Conclusions

In this paper, a control scheme for bilateral teleoperation of a quadrotor has been proposed considering asymmetric and time-varying delays. The structure is formed by a set of P + d controllers in cascade with PID controllers, where only 3 dof of a master device are used for easing to the human operator his remote driving. Besides, the analysis of stability is presented, which gives as result a background for calibrating the damping applied into the system, depending on the time delays added by the communication channel. This result represents the main contribution of the work since encourages even more the use of these known control schemes, addressed to delayed teleoperation of UAV. Finally, human-in-the-loop simulations and experiments of

Please cite this article as: Slawiñski E, et al. Control for delayed bilateral teleoperation of a quadrotor. ISA Transactions (2017), http://dx.doi.org/10.1016/j.isatra.2017.09.021

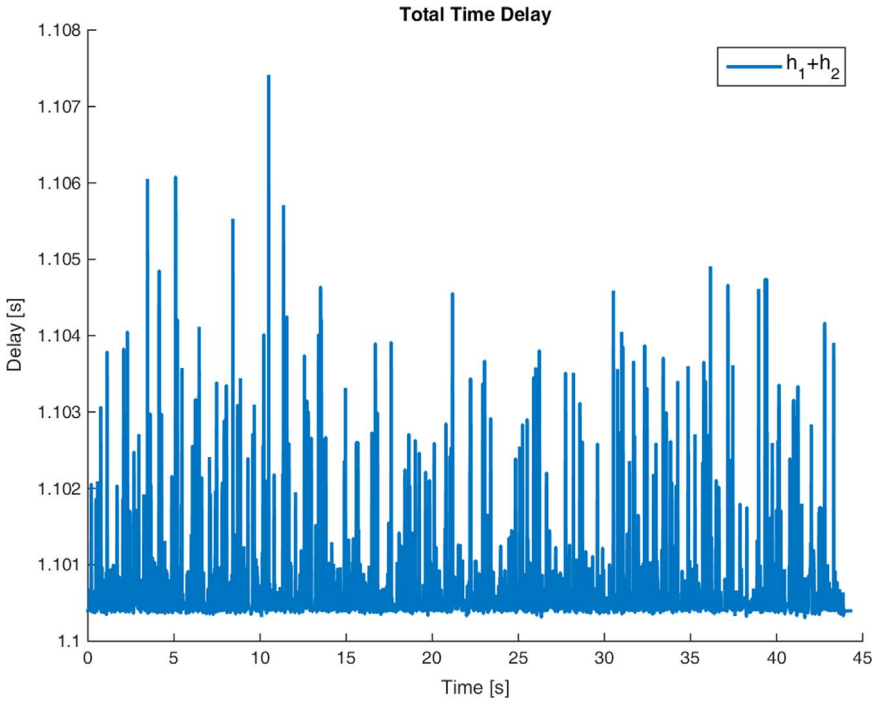

Fig. 8. Round trip delay measured in the test B.

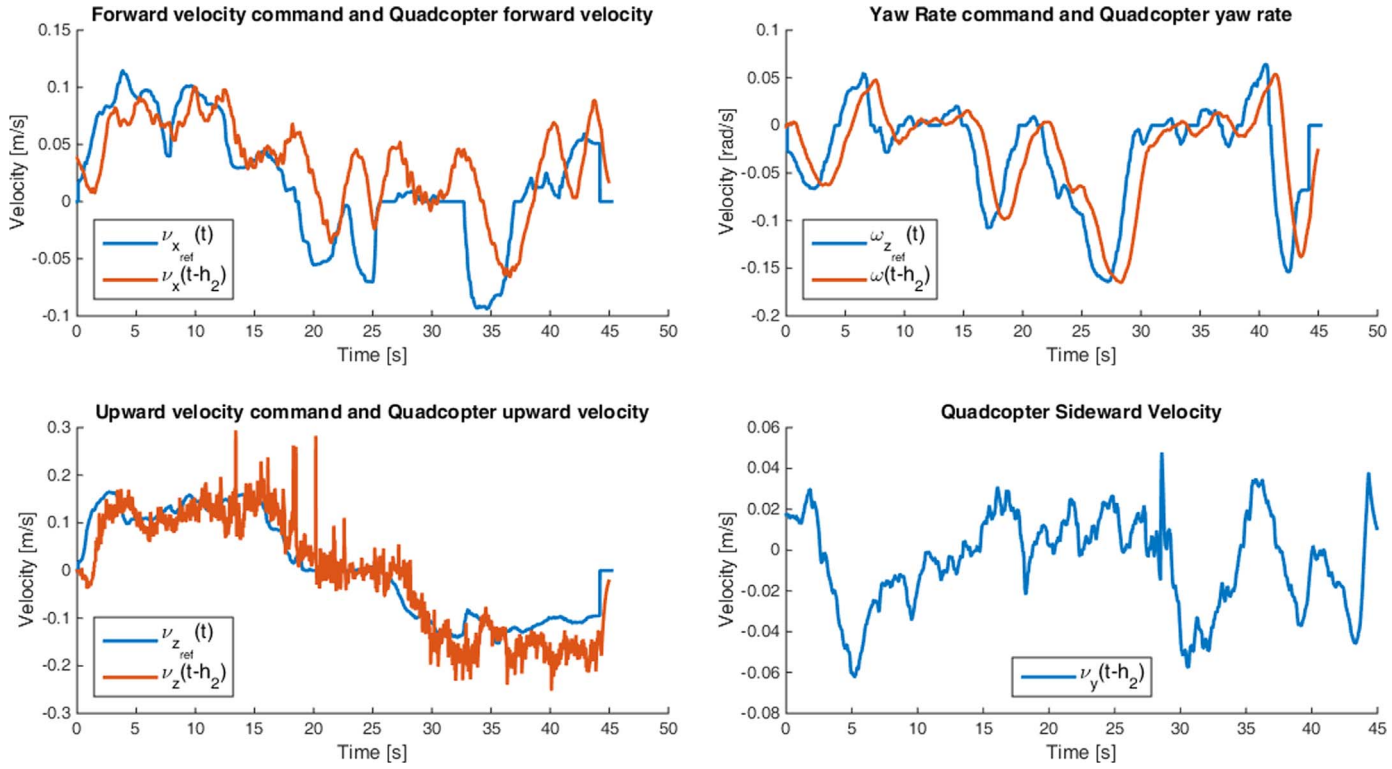

Fig. 9. Evolution of velocity references on the local site and velocities of the quadrotor.

Table 2
Summarized experimental test.

Delay	Synchronization index	Task time
Low Delay	119.7 %	105.2 %
Middle Delay	138.4 %	107.7 %
High delay	185.3 %	120.8 %

delayed teleoperation with a quadrotor were made, whose results about the synchronism error and path followed by the quadrotor, are in agreement with the effect of the damping injected into the system, depending on the time delay. Finally, it is important to remark that the implementation of the control scheme is simple and compatible with the current structure of most autopilots of commercial quadrotors.

Please cite this article as: Slawiñski E, et al. Control for delayed bilateral teleoperation of a quadrotor. ISA Transactions (2017), http://dx.doi.org/10.1016/j.isatra.2017.09.021

Appendix A. Appendix

In this appendix, the derivative of the functional $V = V_1 + V_2 + V_3 + V_4 + V_5 + V_6$ defined in Eqs. (14) to (19) will be developed. First, $\dot{V}_1$ is analyzed from (14) along the master dynamics (1), taking into account **Properties 1** and **2**, as follows,

$$\begin{aligned}\dot{V}_1 &= \frac{1}{2}\dot{\mathbf{x}}_\mathbf{m}^T\dot{\mathbf{M}}_\mathbf{m}\dot{\mathbf{x}}_\mathbf{m} + \dot{\mathbf{x}}_\mathbf{m}^T\mathbf{M}_\mathbf{m}\ddot{\mathbf{x}}_\mathbf{m} - \dot{\mathbf{x}}_\mathbf{m}^T\mathbf{f}_\mathbf{h} \\ &= \frac{1}{2}\dot{\mathbf{x}}_\mathbf{m}^T\dot{\mathbf{M}}_\mathbf{m}\dot{\mathbf{x}}_\mathbf{m} + \dot{\mathbf{x}}_\mathbf{m}^T\mathbf{M}_\mathbf{m}\mathbf{M}_\mathbf{m}^{-1}\left(\mathbf{f}_\mathbf{m} + \mathbf{f}_\mathbf{h} - \mathbf{g}(\mathbf{x}_\mathbf{m}) - \mathbf{C}_\mathbf{m}\dot{\mathbf{x}}_\mathbf{m}\right) - \dot{\mathbf{x}}_\mathbf{m}^T\mathbf{f}_\mathbf{h} \\ &= \dot{\mathbf{x}}_\mathbf{m}^T\left(\mathbf{f}_\mathbf{m} - \mathbf{g}_\mathbf{m}(\mathbf{x}_\mathbf{m})\right)\end{aligned} \tag{37}$$

Next, if the control action $\mathbf{f}_\mathbf{m}$ (11) and the relation (13) are included in (37), it yields,

$$\begin{aligned}\dot{V}_1 =& \dot{\mathbf{x}}_\mathbf{m}^T\Big(-k_m\big(k_g\mathbf{x}_\mathbf{m} - \boldsymbol{\eta}(t-h_2)\big) - \alpha_m\dot{\mathbf{x}}_\mathbf{m} - k_p\mathbf{q}_\mathbf{m}\Big) \\ &= -k_m\dot{\mathbf{x}}_\mathbf{m}^T\big(k_g\mathbf{x}_\mathbf{m} - \boldsymbol{\eta}(t-h_2) + \boldsymbol{\eta} - \boldsymbol{\eta}\big) \\ &\quad - k_p\dot{\mathbf{x}}_\mathbf{m}^T\mathbf{x}_\mathbf{m} - \alpha_m\dot{\mathbf{x}}_\mathbf{m}^T\dot{\mathbf{x}}_\mathbf{m} \\ &= -\alpha_m\dot{\mathbf{x}}_\mathbf{m}^T\dot{\mathbf{x}}_\mathbf{m} - k_m\dot{\mathbf{x}}_\mathbf{m}^T\big(k_g\mathbf{x}_\mathbf{m} - \boldsymbol{\eta}\big) - k_p\dot{\mathbf{x}}_\mathbf{m}^T\mathbf{x}_\mathbf{m} - k_m\dot{\mathbf{x}}_\mathbf{m}^T\int_{t-h_2}^{t}\dot{\boldsymbol{\eta}}(\xi)d\xi \\ &= -\alpha_m\dot{\mathbf{x}}_\mathbf{m}^T\dot{\mathbf{x}}_\mathbf{m} - k_m\dot{\mathbf{x}}_\mathbf{m}^T\big(k_g\mathbf{x}_\mathbf{m} - \boldsymbol{\eta}\big) - k_p\dot{\mathbf{x}}_\mathbf{m}^T\mathbf{x}_\mathbf{m} \\ &\quad - k_m\dot{\mathbf{x}}_\mathbf{m}^T\int_{t-h_2}^{t}\left[\mathbf{z}(\xi) + \gamma k_z\tanh\left(\frac{1}{k_z}\dot{\mathbf{z}}(\xi)\right)\right]d\xi\end{aligned} \tag{38}$$

Following with the ordinary procedure of Lyapunov, $\dot{V}_2$ is obtained from (15) as follows,

$$\begin{aligned}\dot{V}_2 &= \frac{k_m}{k_g}\big(k_g\mathbf{x}_\mathbf{m} - \boldsymbol{\eta}\big)^T\big(k_g\dot{\mathbf{x}}_\mathbf{m} - \dot{\boldsymbol{\eta}}\big) \\ &= k_m\big(k_g\dot{\mathbf{x}}_\mathbf{m} - \boldsymbol{\eta}\big)^T\dot{\mathbf{x}}_\mathbf{m} - \frac{k_m}{k_g}\big(k_g\mathbf{x}_\mathbf{m} - \boldsymbol{\eta}\big)^T\dot{\boldsymbol{\eta}}\end{aligned} \tag{39}$$

Now, $\dot{V}_3$ is computed from (16) of the following manner:

$$\dot{V}_3 = \frac{\alpha_e k_m}{k_s k_g}\boldsymbol{\eta}^T\dot{\boldsymbol{\eta}} \tag{40}$$

Besides, $\dot{V}_4$ along the virtual quadrotor dynamics (10), including $\boldsymbol{\tau}_\mathbf{s}$ (12), the relation between $\boldsymbol{\eta}$ and $\mathbf{z}$ from (13) and $\mathbf{f}_\mathbf{e}$ (8) into the derivative of (17), can be written by:

$$\begin{aligned}\dot{V}_4 &= \frac{k_m}{k_s k_g}\boldsymbol{\eta}^T\mathbf{D}\dot{\boldsymbol{\eta}} \\ &= \frac{k_m}{k_g}\boldsymbol{\eta}^T\big(k_g\mathbf{x}_\mathbf{m}(t-h_1) - \boldsymbol{\eta}\big) - \sigma_s\frac{k_m}{k_s k_g}\boldsymbol{\eta}^T\mathbf{z} + \frac{k_m}{k_s k_g}\boldsymbol{\eta}^T\mathbf{f}_\mathbf{e} \\ &= \frac{k_m}{k_g}\boldsymbol{\eta}^T\big(k_g\mathbf{x}_\mathbf{m}(t-h_1) + k_g\mathbf{x}_\mathbf{m} - k_g\mathbf{x}_\mathbf{m} - \boldsymbol{\eta}\big) \\ &\quad - \sigma_s\frac{k_m}{k_s k_g}\boldsymbol{\eta}^T\mathbf{z} + \frac{k_m}{k_s k_g}\boldsymbol{\eta}^T\mathbf{f}_\mathbf{e} \\ &= \frac{k_m}{k_g}\boldsymbol{\eta}^T\big(k_g\mathbf{x}_\mathbf{m} - \boldsymbol{\eta}\big) - k_m\left(\mathbf{z} + \gamma k_z\tanh\left(\frac{1}{k_z}\dot{\mathbf{z}}\right)\right)^T\int_{t-h_1}^{t}\dot{\mathbf{x}}_\mathbf{m}(\xi)d\xi \\ &\quad - \sigma_s\frac{k_m}{k_s k_g}\mathbf{z}^T\mathbf{z} - \gamma\sigma_s\frac{k_m k_z}{k_s k_g}\mathbf{z}^T\tanh\left(\frac{1}{k_z}\dot{\mathbf{z}}\right) \\ &\quad - \alpha_e\frac{k_m}{k_s k_g}\boldsymbol{\eta}^T\boldsymbol{\eta} + \frac{k_m}{k_s k_g}\boldsymbol{\eta}^T\mathbf{f}_{\mathbf{a}_\mathbf{e}}\end{aligned} \tag{41}$$

Furthermore, $\dot{V}_5$ is obtained from (18) as follows,

$$\dot{V}_5 = k_p\mathbf{x}_\mathbf{m}^T\dot{\mathbf{x}}_\mathbf{m} \tag{42}$$

From (19), and considering Assumption 1, $\dot{V}_6$ can be obtained, using the calculus of the derivative applied to the double integral with time-varying limits, as follows:

$$\begin{aligned}\dot{V}_6 =\ & k_m h_2\mathbf{z}^T\mathbf{z} - k_m\int_{t-h_2}^{t}\mathbf{z}^T(\xi)\mathbf{z}(\xi)d\xi \\ &+ k_m h_1\dot{\mathbf{x}}_\mathbf{m}^T\dot{\mathbf{x}}_\mathbf{m} - k_m\int_{t-h_1}^{t}\dot{\mathbf{x}}_\mathbf{m}^T(\xi)\dot{\mathbf{x}}_\mathbf{m}(\xi)d\xi\end{aligned} \tag{43}$$

The terms with integrals of (43) can be linked with the fourth term of (38) and second term of (41) by using **Lemma 1** (9), obtaining the following relations:

$$\begin{aligned}&- k_m\dot{\mathbf{x}}_\mathbf{m}^T\int_{t-h_2}^{t}\left[\mathbf{z}(\xi) + \gamma k_z\tanh\left(\frac{1}{k_z}\dot{\mathbf{z}}(\xi)\right)\right]d\xi \\ &- k_m\int_{t-h_2}^{t}\mathbf{z}^T(\xi)\mathbf{z}(\xi)d\xi \le \frac{1}{4}h_2 k_m\dot{\mathbf{x}}_\mathbf{m}\dot{\mathbf{x}}_\mathbf{m}\end{aligned} \tag{44}$$

$$\begin{aligned}&- k_m\left[\mathbf{z} + \gamma k_z\tanh\left(\frac{1}{k_z}\dot{\mathbf{z}}\right)\right]^T\int_{t-h_1}^{t}\dot{\mathbf{x}}_\mathbf{m}(\xi)d\xi \\ &- k_m\int_{t-h_1}^{t}\dot{\mathbf{x}}_\mathbf{m}^T(\xi)\dot{\mathbf{x}}_\mathbf{m}(\xi)d\xi \le \frac{1}{4}h_1 k_m\mathbf{z}^T\mathbf{z}\end{aligned} \tag{45}$$

Thus, the terms with integrals of $\dot{V}$ can be replaced by common quadratic terms. Finally, $\dot{V}$ can be built, joining Eqs. (38) to (43) considering also the relations (44) to (45) and neglecting the terms including γ, as follows:

$$\begin{aligned}\dot{V} =\ & \dot{V}_1 + \dot{V}_2 + \dot{V}_3 + \dot{V}_4 + \dot{V}_5 \\ \le\ & \dot{\mathbf{x}}_\mathbf{m}^\mathbf{T}\left[-\alpha_m\mathbf{I} + k_m h_1\mathbf{I} + \frac{k_m}{4}h_2\mathbf{I}\right]\dot{\mathbf{x}}_\mathbf{m} \\ &+ \mathbf{z}^\mathbf{T}\left[-\sigma_s\frac{k_m}{k_s k_g}\mathbf{I} + k_m h_2\mathbf{I} + \frac{k_m}{4}h_1\mathbf{I}\right]\mathbf{z} \\ &+ \frac{k_m}{k_g k_s}\mathbf{z}^\mathbf{T}\mathbf{f}_{\mathbf{a}_\mathbf{e}}\end{aligned} \tag{46}$$

Last relation represents the evolution of $\dot{V}$ along the system trajectories of the delayed teleoperation system of a quadrotor. This result is used in Section 3.1 in order to get a further analysis about the evolution of the main signals of the teleoperation system.

References

[1] Ahmed B, Pota HR, Garratt M. Flight control of a rotary wing uav using backstepping. Int J Robust Nonlinear Control 2010;20(6):639–58.
[2] Stramigioli S, Mahony R, Corke P. A novel approach to haptic tele-operation of aerial robot vehicles. in: Robotics and Automation (ICRA), 2010 IEEE International Conference on, IEEE; 2010. pp. 5302–8.
[3] Kendoul F. Survey of advances in guidance, navigation, and control of unmanned rotorcraft systems. J Field Robot 2012;29(2):315–78.
[4] Lam T, Mulder M, Van Paassen M. Haptic feedback in uninhabited aerial vehicle teleoperation with time delay. J Guid Control Dyn 2008;31(6):1728–39.
[5] Richard J-P. Time-delay systems: an overview of some recent advances and open problems. Automatica 2003;39(10):1667–94.
[6] Slawinski E, Mut VA, Fiorini P, Salinas LR. Quantitative absolute transparency for bilateral teleoperation of mobile robots. IEEE Trans Syst Man Cybern Part A: Syst Hum 2012;42(2):430–42.
[7] Hokayem PF, Spong MW. Bilateral teleoperation: an historical survey. Automatica 2006;42(12):2035–57.
[8] Nuo E, Basaez L, Ortega R. Passivity-based control for bilateral teleoperation: a tutorial. Automatica 2011;47(3):485–95.
[9] Anderson R, Spong MW. Bilateral control of teleoperators with time delay. IEEE Trans Autom Control 1989;34(5):494–501.
[10] Niemeyer G, Slotine J-J. Stable adaptive teleoperation. IEEE J Ocean Eng 1991;16(1):152–62.
[11] Ryu J-H, Artigas J, Preusche C. A passive bilateral control scheme for a teleoperator with time-varying communication delay. Mechatronics 2010;20(7):812–23.
[12] Nuno E, Ortega R, Barabanov N, Basanez L. A globally stable pd controller for bilateral teleoperators. IEEE Trans Robot 2008;24(3):753–8.
[13] Hua C-C, Liu XP. Delay-dependent stability criteria of teleoperation systems with asymmetric time-varying delays. IEEE Trans Robot 2010;26(5):925–32.
[14] Islam S, Liu PX, El Saddik A, Dias J, Seneviratne L. Bilateral shared autonomous

Please cite this article as: Slawiñski E, et al. Control for delayed bilateral teleoperation of a quadrotor. ISA Transactions (2017), http://dx.doi.org/10.1016/j.isatra.2017.09.021

systems with passive and nonpassive input forces under time varying delay. ISA Trans 2015;54:218–28.
[15] Hua C-C, Yang X, Yan J, Guan X-P. On exploring the domain of attraction for bilateral teleoperator subject to interval delay and saturated p + d control scheme. IEEE Transactions on Automatic Control.
[16] Hua C, Yang Y, Liu PX. Output-feedback adaptive control of networked teleoperation system with time-varying delay and bounded inputs. IEEE/ASME Trans Mechatron 2015;20(5):2009–20.
[17] Yang Y, Hua C, Guan X. Finite time control design for bilateral teleoperation system with position synchronization error constrained. IEEE Trans Cybern 2016;46(3):609–19.
[18] Li Z, Xia Y, Wang D, Zhai D-H, Su C-Y, Zhao X. Neural network-based control of networked trilateral teleoperation with geometrically unknown constraints. IEEE Trans Cybern 2016;46(5):1051–64.
[19] Li Z, Xia Y, Sun F. Adaptive fuzzy control for multilateral cooperative teleoperation of multiple robotic manipulators under random network-induced delays. IEEE Trans Fuzzy Syst 2014;22(2):437–50.
[20] Li Z, Xia Y. Adaptive neural network control of bilateral teleoperation with unsymmetrical stochastic delays and unmodeled dynamics. Int J Robust Nonlinear Control 2014;24(11):1628–52.
[21] Ma L, Schilling K. Survey on bilateral teleoperation of mobile robots. In Proceedings of the 13th IASTED international conference on robotics and applications; 2007. pp. 489–94.
[22] Lee D, Spong MW. Passive bilateral teleoperation with constant time delay. IEEE Trans Robot 2006;22(2):269–81.
[23] Park S, Seo C, Kim J-P, Ryu J. Robustly stable rate-mode bilateral teleoperation using an energy-bounding approach. Mechatronics 2011;21(1):176–84.
[24] Van Quang H, Farkhatdinov I, Ryu J-H. Passivity of delayed bilateral teleoperation of mobile robots with ambiguous causalities: Time domain passivity approach. In Intelligent robots and systems (IROS), 2012 IEEE/RSJ international conference on, IEEE; 2012. pp. 2635–40.
[25] Slawiski E, Mut V, Santiago D. Pd-like controller for delayed bilateral teleoperation of wheeled robots. Int J Control 2016:1–24 (just-Accepted).
[26] Giordano PR, Franchi A, Secchi C, Blthoff HH. Experiments of passivity-based bilateral aerial teleoperation of a group of uavs with decentralized velocity synchronization. in: 2011 IEEE/RSJ International conference on intelligent robots and systems, IEEE; 2011. pp. 163–70.
[27] Franchi A, Secchi C, Son HI, Bulthoff HH, Giordano PR. Bilateral teleoperation of groups of mobile robots with time-varying topology. IEEE Trans Robot 2012;28(5):1019–33.
[28] Lee D, Franchi A, Son HI, Ha C, Blthoff HH, Giordano PR. Semiautonomous haptic teleoperation control architecture of multiple unmanned aerial vehicles. IEEE/ASME Trans Mechatron 2013;18(4):1334–45.
[29] Son HI, Franchi A, Chuang LL, Kim J, Bulthoff HH, Giordano PR. Human-centered design and evaluation of haptic cueing for teleoperation of multiple mobile robots. IEEE Trans Cybern 2013;43(2):597–609.
[30] Lee D, Xu D, Feedback r-passivity of lagrangian systems for mobile robot teleoperation. in: Robotics and Automation (ICRA), 2011 IEEE international conference on, IEEE; 2011. pp. 2118–23.
[31] Lee D, Huang K. Passive-set-position-modulation framework for interactive robotic systems. IEEE Trans Robot 2010;26(2):354–69.
[32] Mersha AY, Stramigioli S, Carloni R. On bilateral teleoperation of aerial robots. IEEE Trans Robot 2014;30(1):258–74.
[33] Salinas LR, Slawiski E, Mut VA. Complete bilateral teleoperation system for a rotorcraft uav with time-varying delay. Mathematical Problems in Engineering; 2015.
[34] He Z, Chen Y, Shen Z, Huang E, Li S, Shao Z, Wang Q. Ard-mu-copter: A simple open source quadcopter platform. In: 2015 Proceedings of the 11th international conference on mobile ad-hoc and sensor networks (MSN), IEEE; 015. pp. 158–64.
[35] Kim J, Kang M-S, Park S. Accurate modeling and robust hovering control for a quad-rotor vtol aircraft. In: Selected papers from Proceedings of the 2nd international symposium on UAVs, Reno, Nevada, USA June 810, 2009, Springer; 2009. pp. 9–26.
[36] Santiago DD, Slawiski E, Mut VA. Stable delayed bilateral teleoperation of mobile manipulators. Asian Journal of Control.

Please cite this article as: Slawiñski E, et al. Control for delayed bilateral teleoperation of a quadrotor. ISA Transactions (2017), http://dx.doi.org/10.1016/j.isatra.2017.09.021